ISSN 1070-3284, Russian Journal of Coordination Chemistry, 2015, Vol. 41, No. 12, pp. 805–816. © Pleiades Publishing, Ltd., 2015.
Original Russian Text © P.S. Koroteev, Zh.V. Dobrokhotova, A.B. Ilyukhin, N.N. Efimov, A.V. Gavrikov, V.M. Novotortsev, 2015, published in Koordinatsionnaya Khimiya, 2015, Vol. 41, No. 12, pp. 736–748.

Polymer Lanthanide Cymantrenecarboxylates

P. S. Koroteev*, Zh. V. Dobrokhotova, A. B. Ilyukhin, N. N. Efimov, A. V. Gavrikov, and V. M. Novotortsev

Kurnakov Institute of General and Inorganic Chemistry, Russian Academy of Sciences, Leninskii pr. 31, Moscow, 119991 Russia

**e-mail: pskoroteev@list.ru*

Received July 1, 2015

Abstract—Polymer cymantrenecarboxylate complexes of rare-earth metals, $[Ln(\eta^2\text{-}O_2CCym)_2(\mu\text{-}O_2CCym)_4Ln(ROH)_4]_n \cdot m$Solv (Ln = Nd (**I**), Gd (**II**), Dy (**III**), Ho (**IV**), Er (**V**, **Va**); R = H and Me; Cym = $(\eta_5\text{-}C_5H_4)Mn(CO)_3$; Solv is a solvent molecule), are synthesized by the exchange reactions between $LnCl_3$ and $CymCO_2K$ in aqueous–organic media. Two types of coordination sites alternate in the polymer chain: Ln^{3+} ions coordinating water or methanol molecules and oxygen atoms of the carboxylate anions and Ln^{3+} ions coordinating oxygen atoms of the bridging and chelate carboxylate anions. In both cases, the coordination number of Ln is 8. Polymer $[Dy_4(O_2CCym)_{12}(HOCH_2CH_2OH)_{3.76}(H_2O)_{0.48}]_n \cdot 3n$THF (**VI**) containing four crystallographically independent Dy^{3+} ions is obtained when ethylene glycol is used instead of methanol. The thermal behavior of complexes **I**–**V** in argon and magnetism of complexes **II**, **III**, and **IV** are studied. Complex **III** exhibits the properties of a single-molecule magnet with the chain structure (single-chain magnet) (CIF files CCDC 1410905 (**I**), 1410917 (**II**), 1410906 (**III**), 1410911 (**IV**), 1410918 (**V**), and 1410934 (**VI**)).

DOI: 10.1134/S1070328415120039

INTRODUCTION

The synthesis and study of 3*d*–4*f* heterometallic complexes, in particular, carboxylates, is a wide and intensively developing field of the modern coordination chemistry [1–4]. These compounds have various magnetic, optical, catalytic, and other properties, which makes it possible to use them as a basis of molecular materials with a wide range of functional properties. Heterometallic carboxylates containing a transition metal in the organometallic fragment are rather poorly studied. Mainly ferrocene derivatives have been studied for a long time [5]. We have earlier synthesized and studied the 3*d*–4*f* carboxylates containing the cymantrene ($(\eta^5\text{-}C_5H_5)Mn(CO)_3$) fragment. The most part of these complexes is binuclear, which is typical of lanthanide carboxylates [6–9]. In our previous studies, we also showed the possibility of using the cymantrenecarboxylate fragment as a source of Mn^{2+} ions for the formation of the Mn(II)–Ln(III) complexes [10, 11]. In all cases, the cymantrenecarboxylate complexes consisted of discrete molecules, and no formation of the coordination chain due to the $CymCO_2$ fragments was observed. We synthesized the heteroleptic carboxylate polymers containing the $CymCO_2$ fragments, but the polymer chain of these compounds was formed due to the acetate fragments and the cymantrenecarboxylate residues were arranged at the periphery of the chain [12]. This work is devoted to the synthesis and properties of new organometallic coordination polymers formed due to interaction of lanthanide ions with cymantrenecarboxylate anions in an aqueous–organic medium.

EXPERIMENTAL

The following reagents and solvents were used for the synthesis: hydrated lanthanide chlorides $LnCl_3 \cdot 6H_2O$ (Alfa Aesar), cymantrene (Aldrich), and solvents (MeOH, THF) (Alfa Aesar). Cymantrenecarboxylic acid and ammonium cymantrenecarboxylate were prepared according to known procedures [13, 14]. Prior to use methanol was distilled over magnesium, and THF was distilled over lithium alumohydride. Attenuated total internal reflectance (ATR) IR spectra were recorded in a range of 400–4000 cm^{-1} on a Bruker ALPHA instrument. Microanalyses were carried out on an EA1108 85 Carlo Erba Instruments CHNS analyzer.

Synthesis of $[Nd(\eta^2\text{-}O_2CCym)_2(\mu\text{-}O_2CCym)_4Nd(MeOH)_3(H_2O)]_n \cdot n$MeOH (**I**), $[Ln(\eta^2\text{-}O_2CCym)_2(\mu\text{-}O_2CCym)_4Ln(MeOH)_2(H_2O)_2]_n \cdot n$MeOH $\cdot 0.5n H_2O$ (Ln = Gd (**II**); Ho (**IV**); Er (**V**)), $[Ln(\eta^2\text{-}O_2CCym)_2(\mu\text{-}O_2CCym)_4Ln(H_2O)_4]_n \cdot m$THF (Ln = Dy, $m = 2n$ (**III**); Er, $m = 1.75n$ (**Va**)), and $[Dy_4(O_2CCym)_{12}(HOCH_2CH_2OH)_{3.76}(H_2O)_{0.48}]_n \cdot 3n$THF (**VI**).

Potassium hydroxide (56 mg, 1 mmol) and $CymCO_2H$ (248 mg, 1 mmol) were dissolved in methanol (5 mL). The solution was stirred for 20 min at room temperature. Then a solution of $LnCl_3 \cdot 6H_2O$ (0.33 mmol) in water (6 mL) was added with vigorous

stirring, and THF (7 mL) was added to the reaction mixture. The mixture was refluxed with a reflux condenser in a water bath for 10 min. After cooling, the mixture was filtered through a glass filter and left to evaporate slowly at room temperature in a flask wrapped up with an aluminum foil (to avoid photolysis of the cymantrene fragment). Under these conditions, the products crystallized within a week. The disappearance of the yellow color of the solution indicated the reaction completion. The yields of compounds **I–V** were 65–70%.

Complex **Va** was synthesized in an insignificant yield using an earlier described procedure [6]. Unfortunately, since the amount of the substance was low, we could not characterize it by IR spectroscopy and elemental analysis.

To synthesize complex **VI**, $CymCO_2NH_4 \cdot H_2O$ (142 mg, 0.5 mmol) was dissolved in water (3 mL). A solution of $DyCl_3 \cdot 6H_2O$ (65 mg, 0.17 mmol) in a mixture of water (2 mL) and ethylene glycol (2 mL) was added to the reaction solution with stirring. After THF (6 mL) was added, the mixture was refluxed with a reflux condenser, filtered, and left to evaporate slowly in air as in the cases of the syntheses of complexes **I–V**. The yield of complex **VI** was 64 mg (37%).

For $C_{172}H_{118}O_{103}Mn_{18}Nd_6$ (**I**)

anal. calcd., %:	C, 36.33;	H, 2.09.
Found, %:	C, 36.41;	H, 2.07.

ATR IR for **I** (ν, cm^{-1}): 3658 w, 3623 w, 3350 w, 3108 w, 2018 m, 1913 s, 1593 w, 1553 m, 1528 s, 1478 s, 1395 s, 1362 s, 1218 w, 1198 m, 1106 w, 1061 w, 1037 w, 1017 m, 926 w, 851 w, 820 w, 802 m, 787 m, 664 s, 627 vs, 557 m, 538 s, 490 m, 455 s, 414 m.

For $C_{113}H_{77}O_{69.50}Mn_{12}Gd_4$ (**II**)

anal. calcd., %:	C, 35.39;	H, 2.02.
Found, %:	C, 35.35;	H, 2.01.

ATR IR for **II** (ν, cm^{-1}): 3655 w, 3618 w, 3349 w, 3116 w, 2019 m, 1915 s, 1599 w, 1561 m, 1532 m, 1480 s, 1396 s, 1364 m, 1217 w, 1199 m, 1109 w, 1060 w, 1035 w, 1018 m, 928 w, 851 w, 821 w, 803 m, 787 m, 666 s, 627 vs, 558 m, 538 s, 490 m, 455 s, 413 m.

For $C_{70}H_{64}O_{38}Mn_6Dy_2$ (**III**)

anal. calcd., %:	C, 38.78;	H, 2.98.
Found, %:	C, 38.73;	H, 2.91.

ATR IR for **III** (ν, cm^{-1}): 3348 w, 3227 w, 2018 m, 1910 s, 1678 w, 1600 w, 1562 m, 1532 s, 1480 s, 1396 s, 1361 s, 1307 m, 1199 m, 1174 m, 1105 w, 1061 w, 1034 m, 1017 m, 928 m, 871 w, 852 m, 821 w, 803 m, 786 m, 749 w, 725 w, 706 w, 666 s, 626 vs, 558 m, 537 s, 490 s, 455 s, 415 m.

For $C_{113}H_{77}O_{69.50}Mn_{12}Ho_4$ (**IV**)

anal. calcd., %:	C, 35.11;	H, 2.01.
Found, %:	C, 35.15;	H, 1.97.

ATR IR for **IV** (ν, cm^{-1}): 3655 w, 3614 w, 3384 w, 3200 w, 2017 m, 1907 s, 1602 m, 1563 m, 1535 s, 1478 s, 1395 s, 1362 s, 1199 m, 1105 m, 1059 m, 1038 w, 1017 m, 928 m, 851 m, 844 m, 819 m, 802 m, 785 m, 664 s, 625 vs, 562 s, 537 vs, 489 s, 454 s, 421 m.

For $C_{113}H_{77}O_{69.50}Mn_{12}Er_4$ (**V**)

anal. calcd., %:	C, 35.02,	H, 2.00.
Found, %:	C, 34.99,	H, 1.96.

ATR IR for **V** (ν, cm^{-1}): 3659 w, 3616 w, 3334 w, 3117 w, 2018 m, 1912 s, 1633 w, 1603 w, 1566 m, 1536 s, 1480 s, 1396 s, 1364 s, 1207 m, 1105 w, 1059 w, 1018 m, 928 w, 851 m, 844 m, 823 w, 804 m, 786 m, 666 s, 626 vs, 564 m, 538 s, 489 s, 455 s, 414 m.

For $C_{127.52}H_{95.52}O_{71}Mn_{12}Dy_4$ (**VI**)

anal. calcd., %:	C, 37.60;	H, 2.36.
Found, %:	C, 37.55;	H, 2.33.

ATR IR for **VI** (ν, cm^{-1}): 3247 w, 3114 w, 2955 w, 2852 w, 2018 m, 1915 s, 1556 m, 1536 m, 1480 s, 1392 s, 1362 s, 1316 m, 1198 m, 1068 m, 1031 m, 926 w, 892 w, 878 w, 848 m, 839 m, 802 m, 786 m, 742 w, 726 w, 709 w, 695 w, 664 s, 626 vs, 555 m, 538 s, 496 m, 484 m, 459 s, 436 m, 421 m, 405 m.

The thermal stability of complexes **I–V** was studied by differential scanning calorimetry (DSC) and thermogravimetry (TG). Thermogravimetric measurements in an argon flow (contents of Ar > 99.998%, $O_2 < 0.0002\%$, $N_2 < 0.001\%$, water vapor < 0.0003%, and $CH_4 < 0.0001\%$) (20 mL/min) were carried out on a TG 209 F1 NETZSCH instrument with a heating rate of 10°C/min. The composition of the gas phase was studied on a QMS 403C Aëolos mass spectrometric attachment under the thermogravimetric experimental conditions. The DSC study in a flow of dried artificial air and argon was carried out a DSC 204 F1 NETZSCH calorimeter at a heating rate of 10°C/min. The temperature calibration of the thermobalance and calorimeter was performed by points of phase transitions of standard substances (C_6H_{12}, Hg, KNO_3, In, Sn, Bi, and CsCl; purity 99.99%) according to the standard ISO/CD 11357-1. The thermal analysis data were processed according to the standards ISO 11357-1, ISO 11357-2, ISO 11358, and ASTM E 1269-95 using the NETZSCH Proteus Thermal Analysis package.

X-ray diffraction analysis. Experimental data for complexes **I–III**, **V**, **Va**, and **VI** were collected on a Bruker SMART APEX2 diffractometer ($\lambda(MoK)_\alpha$

radiation, graphite monochromator) [15]. An absorption correction for the crystals of complexes **III**, **V**, and **VI** was applied using the semiempirical method by equivalents (SADABS) [16]. The structures were determined by a combination of a direct method and Fourier syntheses. The site occupancies of the disordered fragments obtained by the isotropic refinement of the structures with fixed thermal parameters of disordered atoms were ignored in subsequent calculations. Structures **III**, **V**, and **VI** were refined by the full-matrix anisotropic–isotropic (for some disordered atoms) least-squares method. Compounds **I**, **II**, and **V** crystallize as druses formed by joints of thin needles. Modulated structures **I**, **II**, and **V** were refined in the three-dimensional approximation, because we could not select single crystals (experimental data were obtained for the joints). For the refinement of structures **I** and **II**, only Ln and Mn atoms were refined anisotropically. In structure **V**, restraints were imposed on the thermal parameters of the anisotropically refined C and O atoms. Complex **IV** is isostructural with complex **II**, which was established by X-ray diffraction analysis.

All calculations were performed using the SHELXS-2014 and SHELXL-2014 programs [17].

The main structural data are presented in Table 1. The experimental data for compounds **I–III**, **V**, **Va**, and **VI** were deposited with the Cambridge Crystallographic Data Centre (CIF files CCDC 1410905, 1410917, 1410906, 1410911, 1410918, and 1410934, respectively; https://summary.ccdc.cam.ac.uk).

RESULTS AND DISCUSSION

Crystalline complexes **I–III** were isolated by the crystallization of exchange products between $CymCO_2K$ and $LnCl_3 \cdot 6H_2O$ (molar ratio 3 : 1) from a water–methanol–THF mixture under conditions implying slow evaporation of the organic phase. Complex **Va** was isolated in an insignificant yield by the crystallization of the product of exchange between $CymCO_2Na$ and $Er(NO_3)_3 \cdot 5H_2O$ (3 : 1) from a THF–toluene–hexane mixture at +4°C. The complexes are yellow crystals (compound **I** (Ln = Nd) has a greenish tint) soluble in DMSO, THF, and pyridine.

Structures **I–III**, **V**, and **Va** are formed by polymer chains $[Ln(\eta^2\text{-}O_2CCym)_2(\mu\text{-}O_2CCym)_4Ln(ROH)_4]_n$ (R = H, Me) and the solvate molecules. The chain structure is topologically the same in all compounds (Fig. 1). The chain unit includes two Ln atoms (one of them coordinates four O atoms of the $\mu\text{-}O_2CCym$ ligands) and four oxygen atoms of ROH. The second Ln atom coordinates four O atoms of the $\mu\text{-}O_2CCym$ ligand and four O atoms of $\eta^2\text{-}O_2CCym$. In isostructural crystals of compounds **III** and **Va**, the Ln atoms lie on axis 2. The chains are additionally strengthened by hydrogen bonds O–H···O, and hydrogen acceptors are the O atoms of the $\mu\text{-}O_2CCym$ and $\eta^2\text{-}O_2CCym$ ligands coordinated by the adjacent Ln atoms. The conjugation between the Cp and COO fragments of O_2CCym results in the approximate planarity of the CpCOO fragment, which predetermines the possibility of isomerism in the unit of the $Ln(\mu\text{-}O_2CCym)_2Ln$ chain, i.e., the possibility of the *cis* and *trans* arrangement of the $Mn(CO)_3$ fragments relatively to the mean plane $Ln(\mu\text{-}O_2CCym)_2Ln$. The projections of the chains onto the plane perpendicular to the polymer chain are shown in Figs. 2a–2c. It is well seen that in compounds **II**, **III**, **V**, and **Va** all fragments have the *trans* structure, whereas in complex **I** one of six crystallographically independent fragments has the *cis* configuration (Fig. 2e). The $Mn(CO)_3$ fragments of ligands $\eta^2\text{-}O_2CCym$ coordinated by one Ln atom in compounds **I–III**, **V**, and **Va** lie at different sides from the mean plane $Ln(\eta^2\text{-}O_2C)_2$. As a whole, all ligands O_2CCym in one chain in structures **II**, **III**, **V**, and **Va** are twisted toward the same direction. The coordination number of the Ln atoms in compounds **I–III**, **V**, and **Va** is 8, and the polyhedron $Ln(\mu\text{-}O_2CCym)_4(ROH)_4$ is a two-capped trigonal prism. The polyhedron $Ln(\eta^2\text{-}O_2CCym)_2(\mu\text{-}O_2CCym)_4$ is strongly distorted because of the formation of two four-membered rings $Ln(\eta^2\text{-}O_2C)$ and is closest to a trigonal dodecahedron, the central sections of trapezohedra of which are occupied by the $\eta^2\text{-}O_2C$ fragments.

Compounds **I**, **II**, and **V** belong to a series of modulated structures $[Ln(\eta^2\text{-}O_2CCym)_2(\mu\text{-}O_2CCym)_4Ln(MeOH)_x(H_2O)_{4-x}]_n \cdot y$MeOH $\cdot z H_2O$. We isolated the single-phase samples of Nd, Gd, Ho, and Er (Fig. 3). The matrix (1/3 –2/3 0 –2/3 –2/3 0 –2/3 –2/3 –1) transforms the unit cell of compound $V = 810$ Å^3 into the cell similar to that of compound **II** with the parameters $a = 17.123$, $b = 19.994$, $c = 20.991$ Å, $\alpha = 74.56°$, $\beta = 83.01°$, $\gamma = 70.88°$ ($V = 6540$ Å^3). The basis cell is halved: $b^* = b/2$. Modulation can be caused by both different ratios of coordinated solvate molecules and *cis,trans*-isomerism of the $Ln(\mu\text{-}O_2CCym)_2Ln$ fragments.

Structure **III** contains two crystallographically independent solvate molecules of THF. The oxygen atom of one of them acts as an acceptor in the O–H···O hydrogen bond, and the second THF molecule is located in a broad cavity and is not involved in the formation of hydrogen bonds. The equivalent thermal parameters of the C and O atoms of the former molecule are $U_{eq} = 0.06–0.09$ Å^2, and the second molecule was refined isotropically: $U_{iso} = 0.10–0.24$ Å^2 (the experimental data were obtained at 150 K). This structure results in easy airing: in crystals of isostructural compound **Va** (the experimental data were obtained at 296 K), the total site occupancy of the "mobile" THF molecule disordered over two positions is 0.75.

We have earlier found that for the crystallization of lanthanide cymantrenecarboxylates in a mixture of THF and 1,2-dimethoxyethane (DME) bidentate DME completely displaces THF from the coordination sphere of lanthanide [9]. In order to study the

Table 1. Main structural data and refinement results for structures **I**–**III**, **V**, **Va**, and **VI**

Parameter	Value					
	I	**II**	**III**	**V**	**Va**	**VI**
T, K	150(2)	120(2)	150(2)	173(2)	296(2)	120(2)
Crystal system	Triclinic	Triclinic	Monoclinic	Triclinic	Monoclinic	Monoclinic
Space group	$P\bar{1}$	$P\bar{1}$	$P2/c$	$P\bar{1}$	$P2/c$	$P2_1/c$
a, Å	21.650(3)	16.879(3)	15.7224(8)	16.944(4)	15.8762(16)	19.1767(9)
b, Å	22.478(6)	19.809(3)	9.8139(5)	19.759(5)	9.8548(10)	27.1472(14)
c, Å	24.838(4)	20.764(4)	25.2866(14)	20.858(6)	25.533(2)	28.0383(13)
α, deg	112.358(5)	76.094(5)	90	76.088(3)	90	90
β, deg	114.113(3)	83.673(5)	96.8560(10)	83.394(3)	95.919(2)	99.804(2)
γ, deg	94.391(5)	72.823(4)	90	72.693(3)	90	90
V, Å^3	9810(3)	6433(2)	3873.8(4)	6464(3)	3973.5(6)	14383.4(12)
Z	2	2	4	2	4	4
ρ_{calcd}, g/cm^3	1.925	1.980	1.859	1.991	1.790	1.881
μ, mm^{-1}	2.772	3.266	2.943	3.795	3.098	3.161
F(000)	5568	3734	2140	3766	2108	7971
Crystal size, mm	0.32 × 0.01 × 0.01	0.25 × 0.005 × 0.005	0.2 × 0.16 × 0.08	0.28 × 0.04 × 0.02	0.28 × 0.2 × 0.13	0.35 × 0.06 × 0.04
θ Range, deg	2.038–23.257	2.058–18.846	2.610–30.590	2.059–23.256	2.217–27.999	2.155–26.091
Index range	$-24 \le h \le 24$, $-24 \le k \le 24$, $-27 \le l \le 27$	$-15 \le h \le 15$, $-17 \le k \le 17$, $-18 \le l \le 18$	$-22 \le h \le 20$, $-14 \le k \le 14$, $-36 \le l \le 34$	$-18 \le h \le 18$, $-21 \le k \le 21$, $-22 \le l \le 23$	$-20 \le h \le 20$, $-13 \le k \le 13$, $-33 \le l \le 33$	$-23 \le h \le 23$, $-33 \le k \le 33$, $-34 \le l \le 29$
Collected reflections	70775	29687	30876	40009	39581	102452
Independent reflections (R_{int})	28133 (0.1281)	10096 (0.1410)	11711 (0.0365)	18456 (0.1120)	9576 (0.0727)	28389 (0.1303)
Restraints/parameters	1/1318	0/877	10/499	1092/1789	133/565	154/1978
Goodness-of-fit	0.938	0.945	1.022	0.954	1.165	0.968
R_1, wR_2 ($I>2\sigma(I)$)	0.0916, 0.2185	0.0726, 0.1562	0.0341, 0.0803	0.0629, 0.1318	0.0541, 0.1325	0.0556, 0.0982
R_1, wR_2 (whole massif)	0.1824, 0.2556	0.1587, 0.1905	0.0574, 0.0895	0.1483, 0.1582	0.1027, 0.1522	0.1485, 0.1264
$\Delta_{max}/\Delta_{min}$, e/Å^3	8.369, −1.859	3.707, −1.234	1.296, −0.868	4.289, −1.800	2.112, −2.403	1.392, −1.645

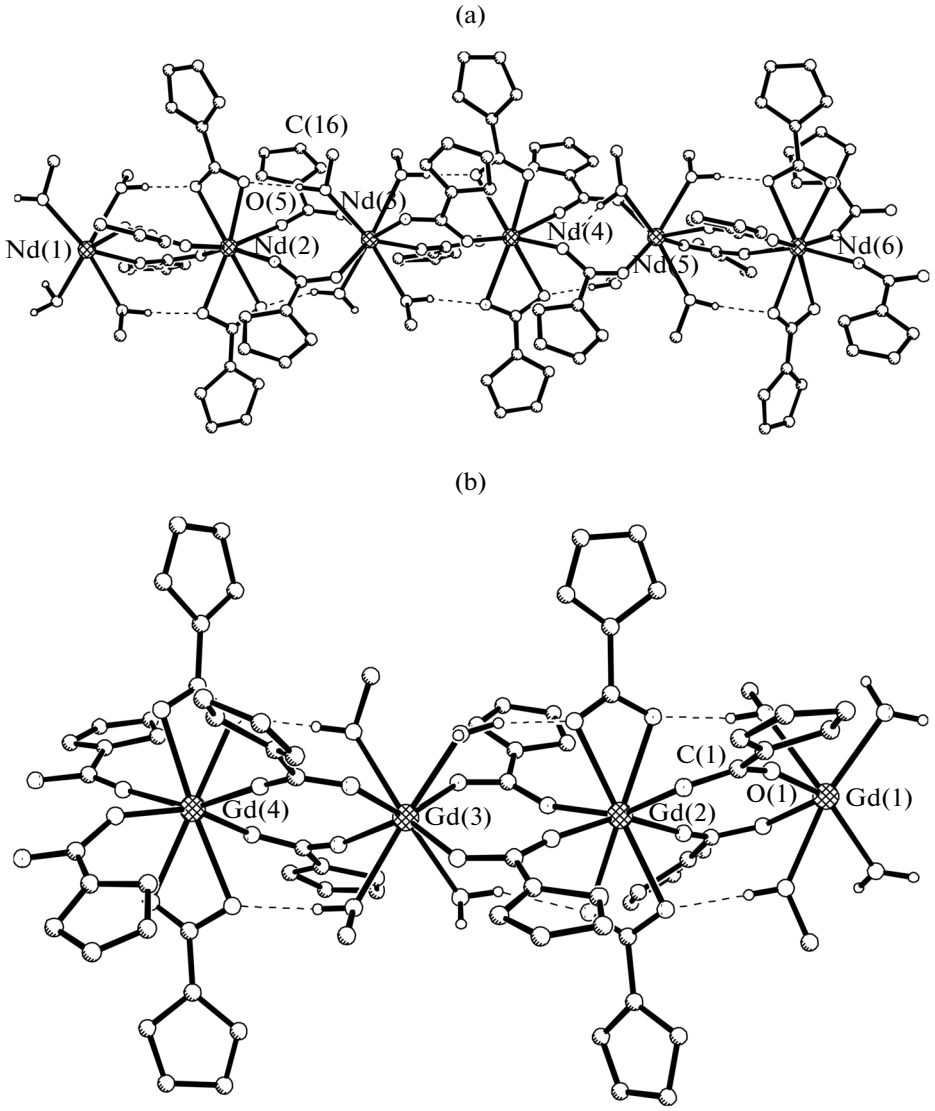

Fig. 1. Structure of the polymer chain in structures (a) **I**, (b) **II**, (c) **III**, and (d) **IV** (fragments $Mn(CO)_3$ are omitted).

influence of the dentate mode of the O ligand on the structure of the product, we carried out a similar exchange reaction between dysprosium chloride and ammonium cymantrenecarboxylate in the presence of bidentate ethylene glycol. It turned out that polymer **VI** was formed in which the most part of water molecules was displaced from the coordination sphere of Dy by ethylene glycol. The formation of a series of coordination polymers $[Ln(L)_3(HOCH_2CH_2OH)]_n$ (L is furan-2-carboxylate; Ln = Nd, Sm, Gd, Tb, Dy, Er) in an aqueous medium in the presence of ethylene glycol, which is the single neutral ligand, has previously been reported [18].

The structure of polymer **VI** contains four crystallographically independent coordination sites. The structure of the polymer chain in compound **VI** is topologically similar to that considered for compounds **I**–**III** and **V** (Fig. 1d), taking into account the replacement of H_2O and MeOH molecules by $HOCH_2CH_2OH$. Figure 2d distinctly shows that, unlike structures **II**, **III**, and **V**, in **VI** the mutual arrangement of the $Mn(CO)_3$ fragments is disordered; moreover, one of the η^2-O_2CCym ligands is disordered over two positions (Fig. 4).

It is most likely that the disorder in structures **I**, **II**, **V**, and **VI** is due to kinetic factors. There are different forms of $Ln_x(O_2CCym)_y(Solv)_z$ in solutions, including dimers with different structures. Complexes complementary to an inoculum are selected in the course of crystal growth. However, the crystal growth rate and the diffusion of a complex with a "suitable" structure can correspond to each other in such a way that the

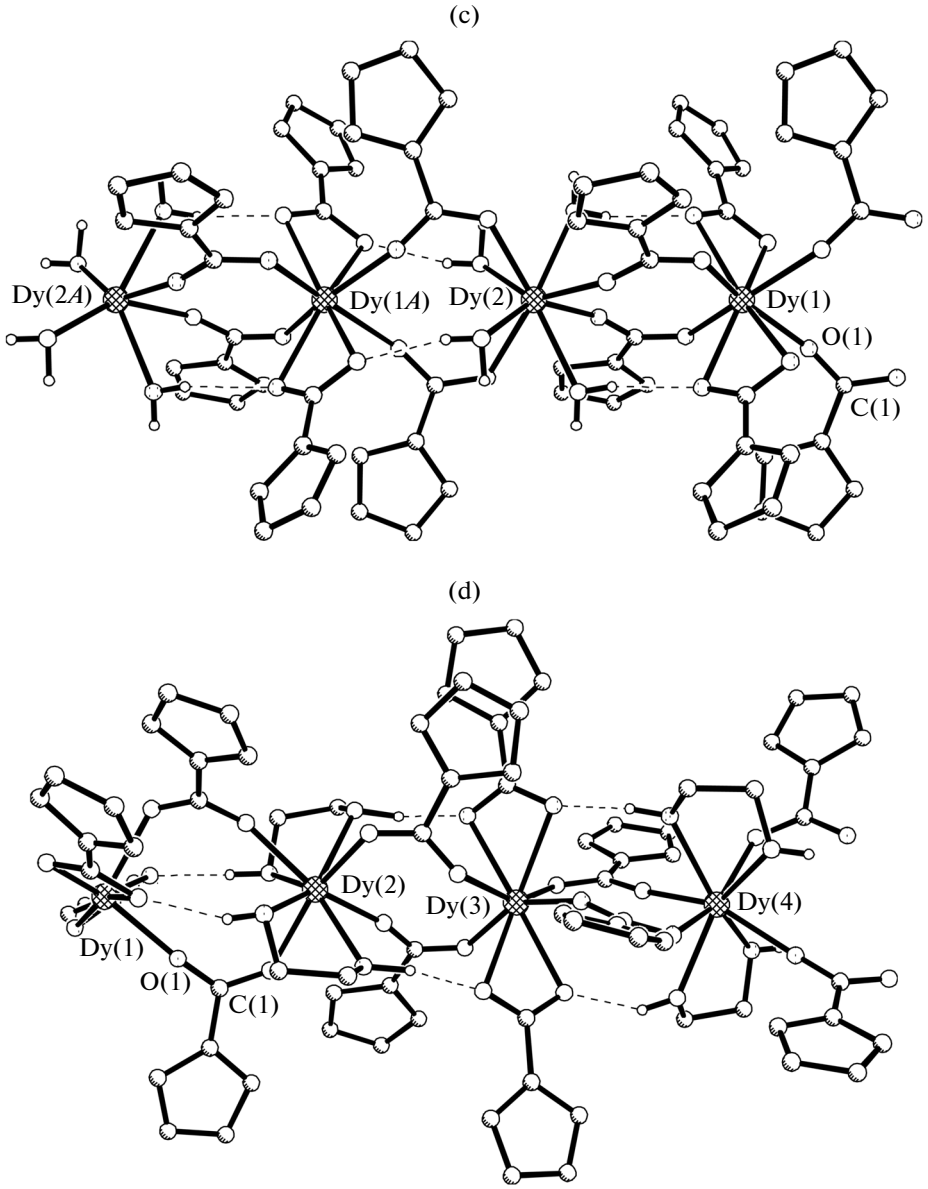

Fig. 1. Contd.

fragment with the structure differed from that of the main chain of the solvate composition (complex **VI**) or the structures of complexes **I** and **VI** can incorporate into the polymer unit. The ordering of defect units results in modulated structures **I**, **II**, and **V**, and their chaotic distribution leads to random disordering (**VI**).

The thermal behavior of complexes **I–V** was carried out in an inert atmosphere in a range of 25–300°C. The thermal decomposition of all studied complexes was nearly similar in the indicated temperature range. The first stage of decomposition of the solvate-free complexes is the removal of coordinated neutral ligands (Table 2).

The removal of the coordinated neutral ligands results in the formation of stable intermediates (to 255 ± 5°C). It was established for all studied complexes that the formed intermediates underwent the reversible phase transition (Fig. 5), whose characteristics are given in Table 2.

It was shown for the earlier studied binuclear complexes $[Ln_2(O_2CCym)_6(THF)_4]$ (Ln = Nd, Eu, Gd) and $[Ln_2(O_2CCym)_6(Py)_4] \cdot 2Py$ (Ln = Pr, Sm, Eu, Gd) that their thermal decomposition occurred similarly and in stages [6, 7]. Intermediates that also undergo the reversible phase transition are formed after the removal of the coordinated neutral ligands.

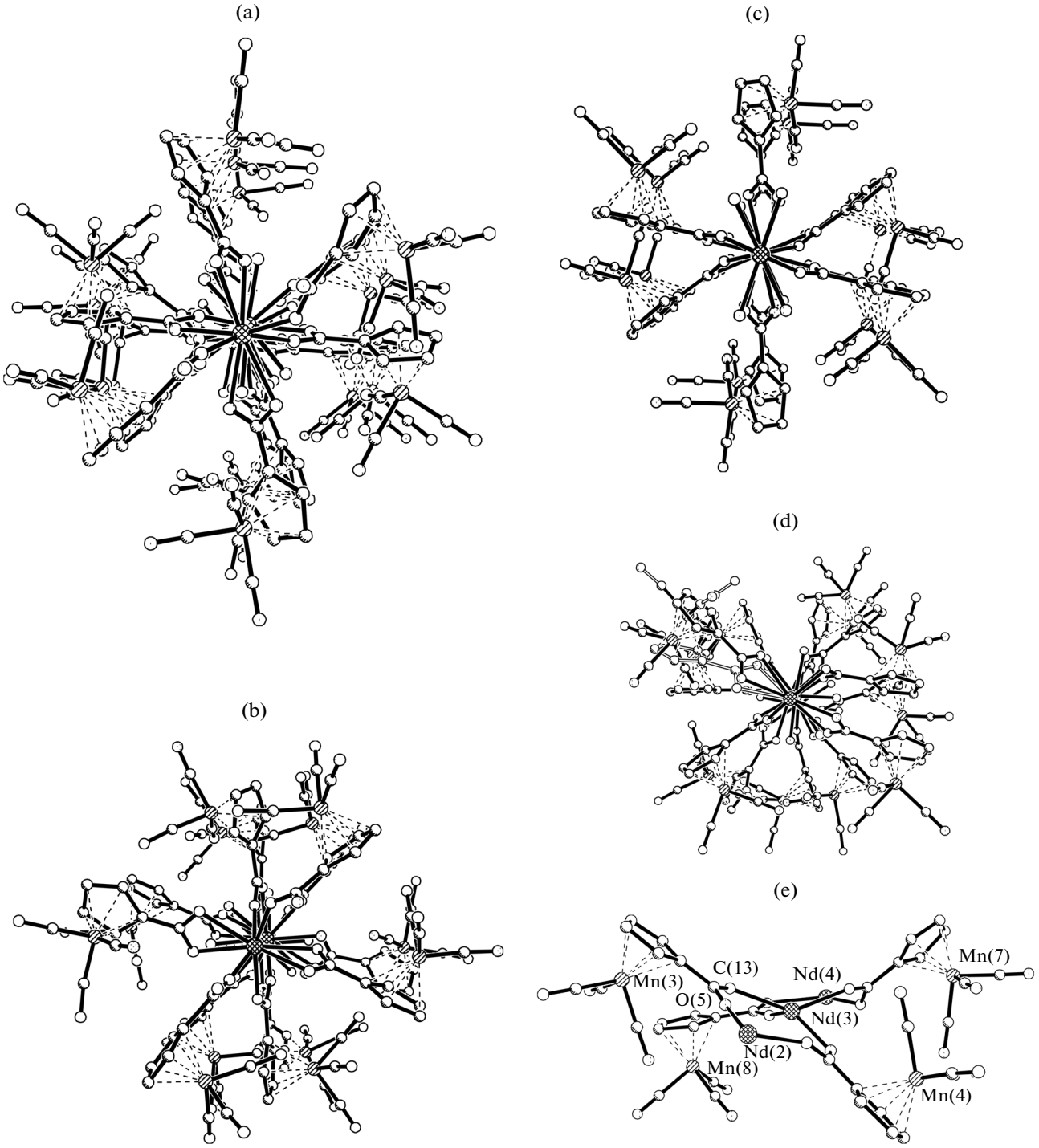

Fig. 2. Projection of the polymer chain along the Ln(1)–Ln(2) vector in structures (a) **I**, (b) **II**, (c) **III**, and (d) **VI** and (e) the fragment of the polymer chain in structure **I**.

The X-ray diffraction studies of the intermediates at two temperatures (25 and 200°C) show that the phase transition is of the first order. The results of thermoanalytical studies suggest an identity of the $\{LnL_3\}$ (L = $CymCO_2$) phases formed at the first stage of thermolysis of both THF- and pyridine-containing binuclear lanthanide cymantrenecarboxylates. It is assumed on the basis of the obtained results (ATR IR spectra) and available published data that the $\{LnL_3\}$ intermediates are carboxylate coordination polymers ($[LnL_3]_n$).

In the case of the thermolysis of complexes **I–V** which are coordination polymers, it can be asserted on

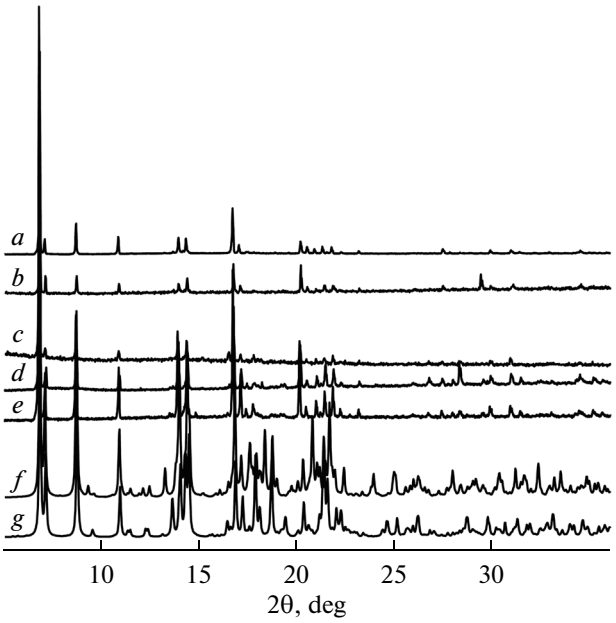

Fig. 3. Experimental ((a) **I**, (b) **II**, (c) **III**, (d) **IV**), and (e) **V**) and theoretical ((f) **I** and (g) **II**) X-ray diffraction patterns of the modulated structures $[Ln(\eta^2\text{-}O_2CCym)_2(\mu\text{-}O_2CCym)_4Ln(MeOH)_x(H_2O)_{4-x}]_n \cdot y$MeOH $\cdot z H_2O$.

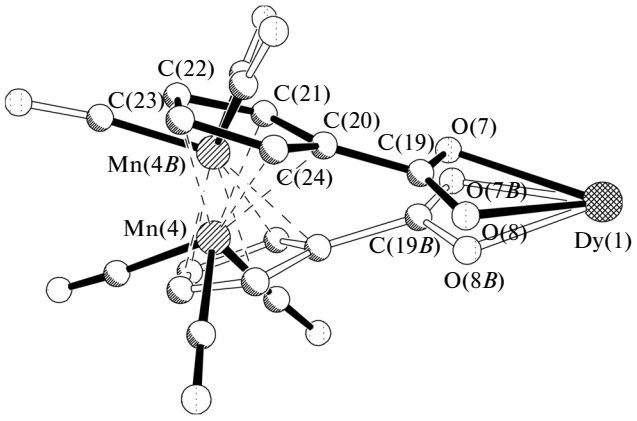

Fig. 4. Structure of the disordered fragment of the polymer chain in structure **VI**.

the basis of the thermal effect of the stage resulting in intermediate formation that no processes leading to polymer chain destruction occur; i.e., the intermediates retain the polymer structure. The comparative study of the IR (ATR) spectra of the initial complexes $[Ln(\mu\text{-}CymCO_2)_6Ln(H_2O)_4]_n$ and phases $[LnL_3]_n$ was performed in order to characterize the structures of the intermediates. When considering the spectra of the carboxylates, the main attention was given to the position of absorption bands assigned to vibrations of carboxyl groups that are most sensitive to changes in the character of anion coordination. The IR spectra of the initial complexes and intermediates exhibit absorption bands characteristic of stretching antisymmetric and symmetric vibrations of the coordinated carboxyl group ($\nu_{as}(COO^-)$ and ($\nu_s COO^-$)) (Fig. 6). The band of antisymmetric vibration $\nu_{as}(COO^-)$ is very sensitive to the coordination mode. The position and complicated character of the $\nu_{as}(COO^-)$ bands in the spectra of the initial complexes (Fig. 6) indicate the different character of the coordination of the carboxyl groups: two bands are observed in ranges of 1527–1533 and 1553–1560 cm^{-1} (for the neodymium, gadolinium, and dysprosium complexes) assigned to $\nu_{as}(COO^-)$. The $\nu_s(COO^-)$ bands for these complexes are observed in a range of 1476–1479 cm^{-1}. The numerical differences $\Delta\nu = \nu_{as}(COO^-) - \nu_s(COO^-)$ are 53 and 80 cm^{-1}, which indicates the presence of chelate and bridging carboxyl groups [19] and is consistent with the results of X-ray diffraction analyses for the initial polymers. In the spectra of the intermediates, the high-frequency band $\nu_{as}(COO^-)$ nearly disappears and the low-frequency band (1530–1533 cm^{-1}) undergoes almost no shift and, hence, the carboxyl groups in the intermediate are more uniform. The change in the coordination mode of the COO groups is also indicated by the changes in the spectrum in the range of bending scissoring and wagging vibrations (Fig. 6). It can unambiguously be asserted that the polymer structure remains unchanged upon the removal of the neutral ligand, but the coordination mode of the carboxyl groups changes in the metal core, with a significant increase in the fraction of chelate-bridging carboxyl groups [19].

Using the present and earlier obtained [6, 7] data on the characteristics of the phase transition of $[LnL_3]_n$, the dependences of the onset temperature and thermal effect of the phase transition on the ion radius of lanthanides were constructed (Fig. 7). It is seen that the quantitative characteristics of the reversible phase transition change monotonically depending on the radius of Ln^{3+}.

Thus, it was established that the removal of volatile neutral ligands from both the new polymer and binuclear cymantrenecarboxylates with the ratio Ln : Mn = 1 : 3 resulted in the formation of polymeric isostructural tris-cymantrenecarboxylates $[Ln(CymCO_2)_3]_n$ that crystallize in the triclinic system, space group $P\bar{1}$ [7].

The magnetic properties of the lanthanide complexes are interesting and promising because of the high magnetic moment and high magnetic anisotropy of certain Ln^{3+} ions, which allows complexes of these metals to serve, in particular, as single-molecule magnets [20, 21]. The temperature dependences of the magnetic susceptibility for complexes **II**, **III**, and **IV** were studied in a range of 300–2 K. For the newly studied complexes **II–IV**, experimentally determined values of $\chi_m T$ at 300 K calculated for the binuclear unit are 15.51, 28.58, and 28.38 $cm^3\ mol^{-1}$ K, which is close to the theoretical values for two isolated Ln^{3+}

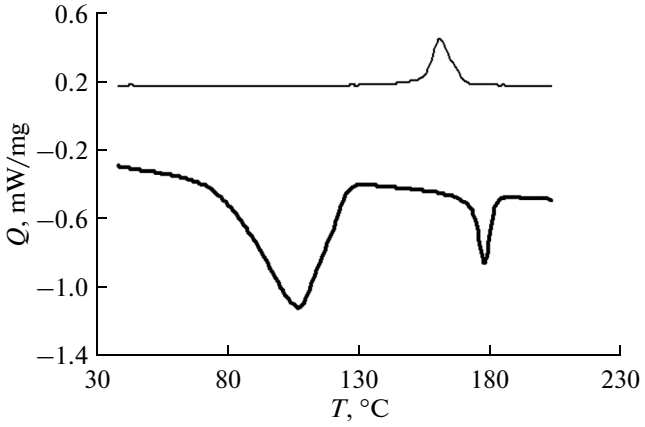

Fig. 5. DSC curves for complex **II** on (—) heating and (—) cooling.

ions (15.76, 28.34, and 28.14 cm^3 mol^{-1} K, respectively [22]).

The magnetic behavior of the compounds containing the Gd^{3+} ion differs from that of the complexes with other lanthanide ions because of specific features of the electronic structure of this ion. First, the Gd^{3+} ion has the maximum possible number of unpaired electrons ($S = 7/2$) in the series of *f* elements. Second, this is isotropic ion having no contribution of the spin-orbital coupling. The value of $\chi_m T$ equal to 15.51 cm^3 mol^{-1} K for complex **II** at room temperature remains unchanged with a temperature decrease to 12 K ($\chi_m T$ (12 K) = 15.70 cm^3 mol^{-1} K), and then a sharp decrease to 8.13 cm^3 mol^{-1} K at 2 K is observed (Fig. 8). The temperature-independent run in a range of 300–12 K is probably due to comparatively weak exchange interactions between the Gd^{3+} ions, which is characteristic of the most part of polynuclear [23] and polymer [24] Gd^{3+} complexes.

For complex **IV**, the value of $\chi_m T$ remains almost unchanged to 150 K and then decreases slowly with the temperature lowering, whereas after attaining ~10 K a sharp drop to 12.5 cm^3 mol^{-1} K at 2 K takes place (Fig. 8). This behavior can be due to the splitting

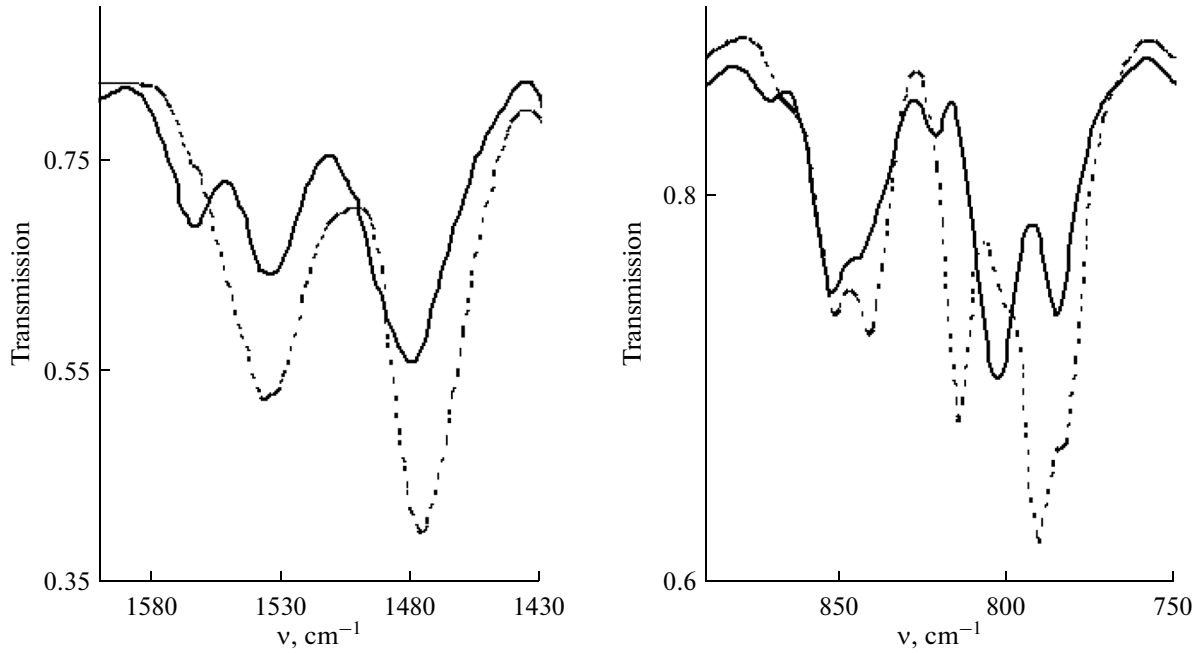

Fig. 6. Fragments of the IR spectra of (—) $[Dy(CymCO_2)_2(\mu\text{-}CymCO_2)_4Dy(H_2O)_4]_n$ and (- - -) $[Dy(CymCO_2)_3]_n$.

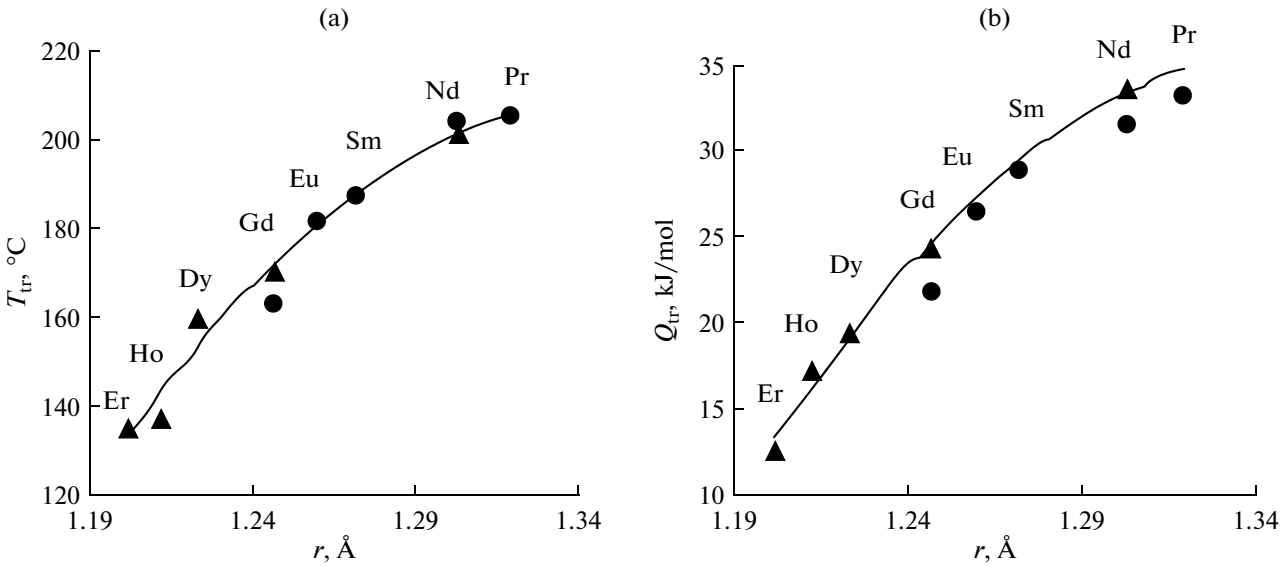

Fig. 7. Dependences of the (a) onset temperature and (b) thermal effect of the phase transition for the intermediate $[Ln(CymCO_2)_3]_n$ on the ion radius of lanthanides: (●) published data [6, 7] and (▲) this work.

in the zero field due to the effect of the ligand field, the Zeeman effect upon external field application, and/or weak antiferromagnetic interactions between lanthanide ions [25].

The temperature dependence $\chi_m T$ is somewhat different for complex **III** but is similar to that observed earlier [26]. The value of $\chi_m T$ at 300 K almost coincides with the theoretical value for the Dy^{3+} ion ($S = 5/2$, L = 5, $^6H_{15/2}$, $g = 4/3$). As the temperature decreases, $\chi_m T$ somewhat increases reaching 30.02 cm^3 mol^{-1} K at 61 K and then decreases to 18.5 cm^3 mol^{-1} K at 2 K. It can be assumed that an increase in $\chi_m T$ is due to the intramolecular ferromagnetic exchange between the Dy^{3+} ions in the chain, whereas a decrease in $\chi_m T$ with the temperature lowering is related to a decrease in the occupancy of the excited m_J sublevels, the Zeeman effect upon external field application, and/or antiferromagnetic interactions between the Dy^{3+} ions in the adjacent chains.

The ability of the lanthanide complexes to manifest molecular magnetism is especially interesting. It is known that the Dy^{3+} ion is one of the most suitable for the design of single-molecule magnets, since this ion is highly anisotropic and has an odd number of electrons, i.e., this is Kramer's ion and its state is bistable regardless of the field of ligands. Thus, both conditions necessary for the appearance of molecular magnetism are optimally combined in the case of dysprosium [27, 28]. The susceptibility of complex **III** was measured in an alternating field to determine its ability to serve as a single-molecule magnet. A maximum is observed in the zero external field on the frequency dependences of the imaginary component χ" at low temperatures of 2–3 K, which demonstrates the slow relaxation of magnetization and the behavior of a single-molecule magnet (Fig. 9). The relaxation time ($\tau(T_{max}) = 1/(2\pi\nu)$) was obtained by measurements of the isotherms of the frequency dependences. Figure 10 shows the dependence of $\ln\tau$ on the inverse temperature ($1/T$) for a range of 2.0–3.5 K. The preexponential factor $\tau_0 = 4.3 \times 10^{-6}$ s and the energy barrier for relaxation $\Delta E/k = 4.1$ K were determined using the Arrhenius law $\tau = \tau_0 \exp(\Delta E/kT)$. The shape of the dependence of $\ln\tau$ on $1/T$ suggests that relaxation is thermally activated and the purely quantum mode occurs below the temperature of the study ($T < 2$ K).

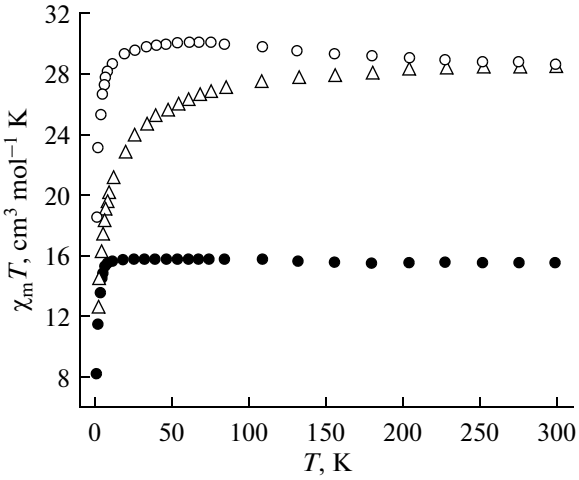

Fig. 8. Dependences $\chi_m T(T)$ for complexes (●) **II**, (○) **III**, and (△) **IV**.

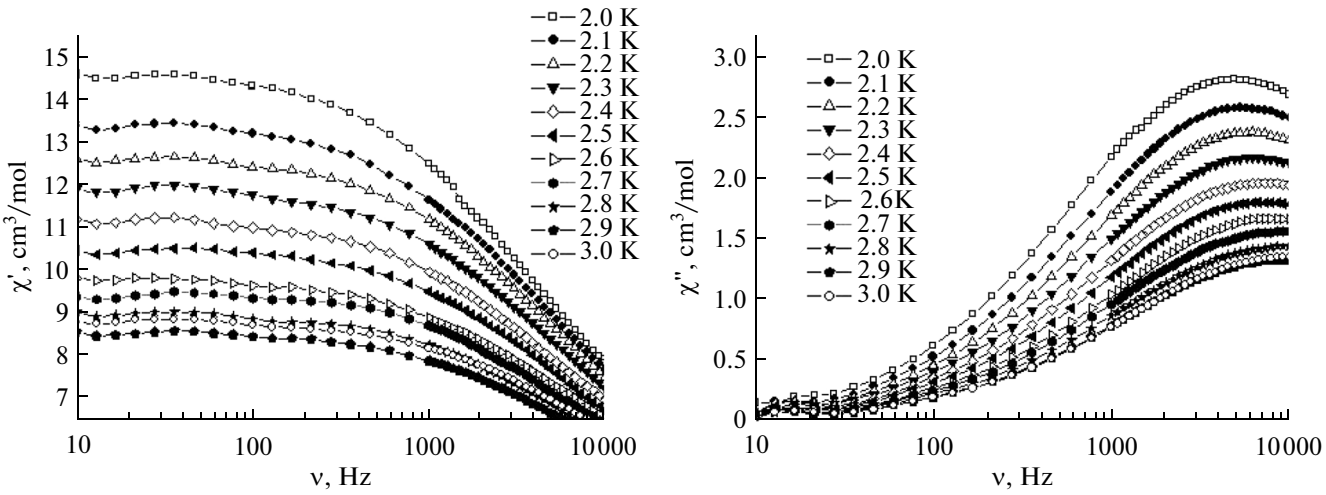

Fig. 9. Frequency dependences of the (left) real and (right) imaginary parts of the dynamic magnetic susceptibility of the sample of complex **III** ($H_{DC} = 0$ Oe).

The symmetrical shape of the χ''(χ') plots (Cole–Cole diagram) (Fig. 11) confirms that in a range of 2–3.5 K relaxation is thermally activated with the single parameter τ_0.

Thus, we showed that polymer chains are formed of lanthanide ions and cymantrenecarboxylate anions in aqueous–organic media, unlike media of aprotic solvents. In the structures of the formed polymers, the coordination sites regularly alternate in which the Ln ions are coordinated by either solvent molecules and oxygen atoms of bridging carboxylates, or exclusively carboxylate oxygen atoms belonging to the chelating and bridging groups. The use of bidentate ethylene glycol instead of methanol results, to a significant extent, in the substitution of water by the bidentate ligands, and the structure of the polymer becomes more complicated. The staged character of thermolysis of the coordination polymers and the polymer nature of the intermediates formed after the removal of volatile ligands were established. The magnetic properties of the complexes containing highly paramagnetic lanthanide ions were studied. The Dy complex was found to exhibit the properties of a single-molecule magnet.

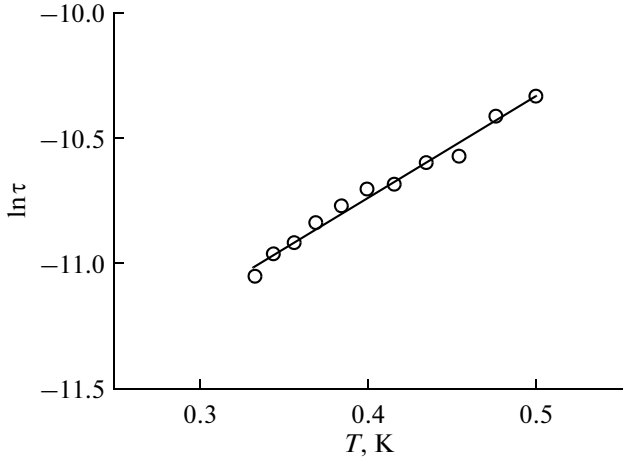

Fig. 10. Dependence of lnτ on $1/T$ for the sample of complex **III** obtained from the frequency dependences of χ'' in the zero magnetic field.

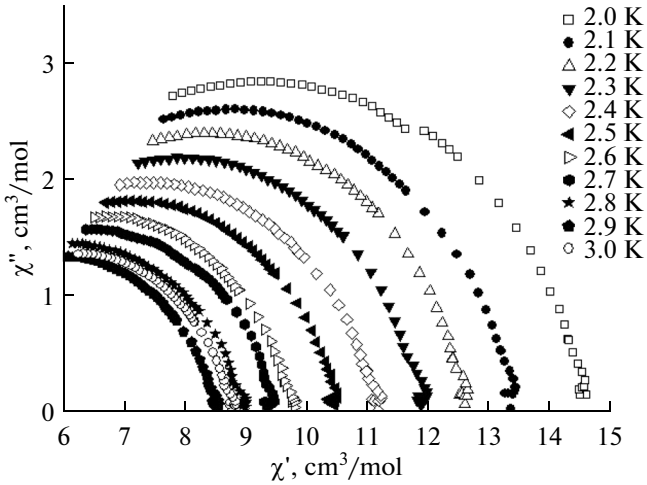

Fig. 11. Cole–Cole diagram for complex **III** (H_{DC} = 0 Oe).

Table 2. Characteristics of the first stage of thermolysis of complexes **I**–**V** in argon (heating rate 10 deg/min)

Characteristic	**I**	**II**	**III**	**IV**	**V**
$T_{onset} \pm 2.0$, °C	78.0	75.5	76.0	74.8	78.9
$T_{fin.\ 1\ stage}$, °C	112.3	120.0	108.4	107.0	107.2
$Q_{1\ stage} \pm 5.0$ (endo), kJ/mol	213.3	237.8	236.5	225.4	230.3
$\Delta m_{1\ stage} \pm 1.5$, %	7.2	5.9	4.6	5.2	5.9
% of ROH content ROH (R = H, Me)	8.36	6.79	4.02	6.76	6.75
$T_{transition} \pm 2.0$, °C	201.7 203.9*	170.2 162.8*	159.8	137.0	135.0
$Q_{transition} \pm 4.0$, kJ/mol	33.4 31.3*	24.2 21.7*	19.3	17.2	12.5

* Data obtained in [6, 7].

ACKNOWLEDGMENTS

This work was supported by the Russian Science Foundation, project no. 14-13-00938.

REFERENCES

1. Masatomi, S., Kazuhiro, M., and Hisashi, O., *Coord. Chem. Rev.*, 2001, vols. 219–221, p. 379.
2. Andruh, M., Costes, J.-P., Diaz, C., and Gao, S., *Inorg. Chem.*, 2009, vol. 48, p. 3342.
3. Huang You-Gui, Jiang Fei-Long, and Hong Mao-Chun, *Coord. Chem. Rev.*, 2009, vol. 253, p. 2814.
4. Sharples, J.W. and Collison, D., *Coord. Chem. Rev.*, 2014, vol. 260, p. 1.
5. Koroteev, P.S., Dobrokhotova, Zh.V., Efimov, N.N., et al., *Russ. J. Coord. Chem.*, 2014, vol. 40, no. 7, p. 495.
6. Koroteev, P.S., Kiskin, M.A., Dobrokhotova, Zh.V., et al., *Polyhedron*, 2011, vol. 30, p. 2523.
7. Koroteev, P.S., Dobrokhotova, Zh.V., Kiskin, M.A., et al., *Polyhedron*, 2012, vol. 43, p. 36.
8. Koroteev, P.S., Dobrokhotova, Zh.V., Ilyukhin, A.B., et al., *Izv. Akad. Nauk, Ser. Khim.*, 2012, no. 6, p. 1064.
9. Koroteev, P.S., Dobrokhotova, Zh.V., Ilyukhin, A.B., et al., *Polyhedron*, 2013, vol. 65, p. 110.
10. Koroteev, P.S., Efimov, N.N., Ilyukhin, A.B., et al., *Inorg. Chim. Acta*, 2014, vol. 418, p. 157.
11. Koroteev, P.S., Efimov, N.N., Dobrokhotova, Zh.V., et al., *Russ. J. Coord. Chem.*, 2015, vol. 41, no. 3, p. 149.
12. Koroteev, P.S., Dobrokhotova, Zh.V., Ilyukhin, A.B., et al., *Polyhedron*, 2015, vol. 85, p. 941.
13. Nesmeyanov, A.N., Anisimov, K.N., Kolobova, N.E., and Makarov, Yu.V., *Izv. Akad. Nauk SSSR, Ser. Khim.*, 1968, no. 3, p. 686.
14. Ilyukhin, A.B., Koroteev, P.S., Kiskin, M.A., et al., *J. Mol. Struct.*, 2013, vol. 1033, p. 187.
15. *APEX2 and SAINT*, Madison (WI, USA): Bruker AXS Inc., 2007.
16. Sheldrick, G.M., *SADABS*, Göttingen (Germany): Univ. of Göttingen, 1997.
17. Sheldrick, G.M., *Acta Crystallogr., Sect. A: Found. Crystallogr.*, 2008, vol. 64, no. 1, p. 112.
18. Ying Wang, Xi-Li Li, Tian-Wei Wang, et al., *Inorg. Chem.*, 2010, vol. 49, p. 969.
19. Deacon, G.B. and Phillips, R.J., *Coord. Chem. Rev.*, 1980, vol. 33, p. 227.
20. Sorace, L., Benelli, C., and Gatteschi, D., *Chem. Soc. Rev.*, 2011, vol. 40, p. 3092.
21. Feltham, H.L.C. and Brooker, S., *Coord. Chem. Rev.,* 2014, vol. 276, p. 1.
22. Benelli, C. and Gatteschi, D., *Chem. Rev.*, 2002, vol. 102, p. 2369.
23. Sourav, D., Atanu, D., Sourav, B., et al., *Inorg. Chem.*, 2014, vol. 53, p. 3417.
24. Koroteev, P.S., Efimov, N.N., Dobrokhotova, Zh.V., et al., *Izv. Akad. Nauk, Ser. Khim.*, 2013, no. 8, p. 1768.
25. Goura, J., Walsh, J.P.S., Tuna, F., and Chandrasekhar V., *Inorg. Chem.*, 2014, vol. 53, p. 3385.
26. Hussain, B., Savard, D., Burchell, T.J., et al., *Chem. Commun.*, 2009, no. 9, p. 1100.
27. Peng Zhang, Yun-Nan Guo, and Jinkui Tang, *Coord. Chem. Rev.*, 2013, vol. 257, p. 1728.
28. Woodruff, D.N., Winpenny, R.E.P., and Layfield, R.A., *Chem. Rev.*, 2013, vol. 113, p. 5110.

Translated by E. Yablonskaya